

---

# Inference, Learning and Attention Mechanisms that Exploit and Preserve Sparsity in Convolutional Networks

---

Timo Hackel<sup>1</sup> Mikhail Usvyatsov<sup>1</sup> Silvano Galliani<sup>1</sup> Jan D. Wegner<sup>1</sup> Konrad Schindler<sup>1</sup>

## Abstract

While CNNs naturally lend themselves to densely sampled data, and sophisticated implementations are available, they lack the ability to efficiently process sparse data. In this work we introduce a suite of tools that exploit sparsity in both the feature maps and the filter weights, and thereby allow for significantly lower memory footprints and computation times than the conventional dense framework when processing data with a high degree of sparsity. Our scheme provides (i) an efficient GPU implementation of a convolution layer based on direct, sparse convolution; (ii) a filter step within the convolution layer, which we call *attention*, that prevents fill-in, i.e., the tendency of convolution to rapidly decrease sparsity, and guarantees an upper bound on the computational resources; and (iii) an adaptation of the back-propagation algorithm, which makes it possible to combine our approach with standard learning frameworks, while still exploiting sparsity in the data and the model.

## 1. Introduction

Deep neural networks are nowadays the most popular and most successful tool for a wide spectrum of computer vision problems (Krizhevsky et al., 2012; Long et al., 2015; Ren et al., 2015). A main reason for their spectacular comeback, perhaps even the single most important factor besides much larger training data sets, is the enormous gain in computational efficiency brought about by highly efficient parallel computing on GPUs. Both the response maps (feature maps) within the neural network and the parameters (filter weights) of the network form regular grids that are conveniently stored and processed as tensors. However, when going beyond standard image processing tasks, regular grids can be a somewhat unnatural and suboptimal representation,

<sup>1</sup>Institute of Geodesy and Photogrammetry, ETHZ, Zurich, Switzerland. Correspondence to: Timo Hackel <timo.hackel@geod.baug.ethz.ch>.

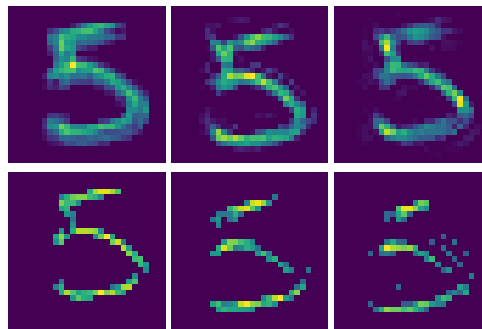


Figure 1. Activations for one channel of the first, second and third convolutional layers after one training epoch, in a neural network for MNIST digit classification. *Top*: dense network; *Bottom*: sparse network with upper bound of  $\rho_{up} = 15\%$  density per channel

for instance for decentralised multi-sensor systems, or for unstructured 3D point clouds.

Typically, point clouds are acquired with line-of-sight instruments, thus the large majority of points lies on a small number of 2D surfaces. When represented as a 3D voxel grid they therefore exhibit a high degree of sparsity: most voxels are empty; while at the same time 3D data processing with CNNs is seriously challenged by the high memory demands (Brock et al., 2016; Wu et al., 2015a; Maturana & Scherer, 2015; Huang & You, 2016). A counter-measure is to make explicit the sparsity of the feature maps, (see example in Figure 1). One way to do this is to change the data representation, e.g., (Riegler et al., 2017) use an octree instead of regular voxels. Another possibility is to store the voxel grids as sparse tensors, usually implemented as compressed sparse rows (CRS) or index-value pairs.

It can also be beneficial to represent the CNN parameters in a sparse fashion. This can potentially improve both runtime and – perhaps more important for modern, deep architectures – memory footprint; especially if the sparsity is promoted already during training through appropriate regularisation. It is obvious that, in a sufficiently sparse setting, a significant speed-up can be achieved by performing convolutions *directly*, incrementally updating a layer’s output map only where there are non-zero entries in the input map as well as non-zero filter weights. This has recently been con-

firmed independently by two concurrent works (Engelcke et al., 2017; Park et al., 2017). Direct convolution guarantees that only the minimum number of necessary operations is carried out. However, the selective, incremental updating only at indexed locations makes parallelisation harder. This may be the reason why, to our knowledge, no practical implementation with sparse feature maps exist (in (Park et al., 2017), a smaller gain is achieved by storing only the filter weights in CRS format). In this work we develop a framework to exploit both sparse feature maps and sparse filter parameters in CNNs. To that end (i) we provide a sparse *Direct Convolution Layer*, as well as sparse versions of the *ReLU* and *max-pooling* layers; (ii) we extend the back-propagation algorithm to preserve sparsity and make our sparse layers usable with existing optimization routines that are available in modern deep learning frameworks, which have been designed for dense data; (iii) we propose to add a density-dependent regulariser that encourages sparsity of the feature maps, and a pruning step that suppresses small filter weights. This regularisation in fact guarantees that the network gets progressively faster at its task, as it receives more training. All these steps have been implemented on GPU as extensions of *Tensorflow*, for generic  $n$ -dimensional tensors. Source code and data are publicly available<sup>1</sup>. We test our sparse CNN structure both on a sparse version of MNIST and on realistic 3D data sets, and show that it outperforms its dense counterpart in terms of both runtime and memory footprint when processing data with a high degree of sparsity.

## 2. Related Work

**Dense CNN for sparse data.** Neural networks, usually of the deep, convolutional network flavour, offer the possibility to completely avoid heuristic feature design and feature selection. They are at present immensely popular in 2D image interpretation. Recently, deep learning pipelines have been adapted to voxel grids (Prokhorov, 2010; Lai et al., 2014; Maturana & Scherer, 2015; Wu et al., 2015b), RGB-D images (Song & Xiao, 2016) and video (Karpathy et al., 2014), too. Being completely data-driven, these techniques have the ability to capture appearance (intensity patterns) as well as geometric object properties. Moreover, their multi-layered, hierarchical architecture is able to encode a large amount of contextual information. A general drawback when directly applying 3D-CNNs to (dense) voxel grids derived from (originally sparse) point clouds is the huge memory overhead for encoding empty space. Computational complexity grows cubically with respect to voxel grid resolution, but in fact high resolution would only be needed at object surfaces.

**Data sparsity.** Therefore, more recent 3D-CNNs exploit the *sparsity of occupied voxels* prevalent in practical voxel grids. Graham et al. (Graham, 2014) introduced a sparse CNN, which takes into account sparsity but is limited to small resolutions due to decreasing sparsity in convolutional layers. In their publication they consider resolutions of up to  $80^3$  voxels. Another strategy is to resort to an octree representation, where empty space (and potentially also large, geometrically simple object parts) are represented at coarser scales than object details (Riegler et al., 2017; Tatarchenko et al., 2017). Since the octree partitioning is a function of the object at hand, an important question is how to automatically adapt to new, previously unseen objects at test time. While (Riegler et al., 2017) assume the octree structure to be known at test time, (Tatarchenko et al., 2017) learn to predict the octree structure together with the labels. This allows generalization to unseen instances of a learned object category, without injecting additional prior knowledge. Häne et al. (Häne et al., 2017) uses a coarse-to-fine scheme to hierarchically predict the values of small blocks of voxels in a voxel block octree. Another strategy is to rely only on a small subset of the most discriminative points, while neglecting the large majority of less informative ones (Li et al., 2016; Qi et al., 2017a;b). The idea is that the network learns how to select the most informative points from training data and aggregates information into global descriptors of object shape via fully-connected layers. This allows for both shape classification and per-point labeling, while using only a small subset of points, resulting in significant speed and memory gains. Recently, Graham et al. (Graham & van der Maaten, 2017; Graham et al., 2017) advocate the strategy to perform convolutions only on non-zero elements in the feature map and find correspondences with the help of hash tables. However, to limit activations to non-zero elements of the input can increase the error and slow down learning.

**Parameter sparsity.** Several works address the situation that the model *parameters* are sparse. Denil et al. (Denil et al., 2013) reduce the network parameters by exploiting low rank matrix factorization. Liu et al. (Liu et al., 2015) exploit the decomposition of matrices to perform efficient convolutions with sparse kernel parameters. Jaderberg et al. (Jaderberg et al., 2014) as well as Denton et al. (Denton et al., 2014) approximate convolutional filters to achieve a faster runtime. Han et al. (Han et al., 2015) use connection pruning to reduce the number of network parameters. Wen et al. (Wen et al., 2016) reduce the parameters of a pre-trained network with structured sparsity learning.

**Direct Convolutions.** The works of Park et al. (Park et al., 2017), Engelcke et al. (Engelcke et al., 2017) and Parashar et al. (Parashar et al., 2017) are the most related ones to our approach, in that they also perform convolutions in a

<sup>1</sup><https://github.com/TimoHackel/ILA-SCNN>

direct manner to efficiently exploit sparseness in network parameters and feature maps. While Park *et al.* use compressed rows as sparse tensor format for the filter parameters, neither (Engelcke *et al.*, 2017) nor (Park *et al.*, 2017) uses a sparse tensor format for both filter parameters and feature maps. Parashar *et al.* (Parashar *et al.*, 2017) implement sparse convolutions on a custom-designed hardware to achieve an energy- and memory-efficient deep CNN. Note that even though all three works follow a similar idea, only Parashar *et al.* exploit sparsity in both the parameters and the data, with compressed sparse blocks, but require dedicated, non-standard hardware.

### 3. Method

At a conceptual level, it is a general theme of computing to speed up computations and reduce memory usage by exploiting sparsity in the data. In the following section, we propose a number of ways to do the same for the specific case of neural network layers, always keeping in mind the specific requirements and limitations of modern GPU architectures. Throughout, sparse tensors are represented and manipulated in a format similar to *Coordinate List*<sup>2</sup>, which stores indices into the sparsely populated grid and the corresponding data entries in separate tensors, and is available in the “SparseTensor” implementation of *Tensorflow*. To minimise memory overhead, the indices of the form  $\{batch, index_x, index_y, \dots, channel\}$  are compressed into unique 1D keys and only expanded when needed.

In order to achieve coalesced memory access, which permits efficient caching and thus fast memory access, the tensors for feature maps are sorted w.r.t. batches and within each batch w.r.t. channels. Likewise, filter weights are sorted w.r.t. the output channels and within each channel w.r.t. the input channels. Compared to dense tensors, the sparse representation naturally adds some overhead. For instance, in our implementation we use 64 bit keys, and 32 bit depth for feature maps. Consequently, storing a dense feature map (100% density) required  $3\times$  more memory. For densities  $<33\%$  the sparse representation is more efficient, and at low densities the savings can be quite dramatic, e.g., at density 1% the sparse version uses 97% less memory.

#### 3.1. Sparse Convolution

Our convolutional layer is designed to work with sparse tensors for both feature maps and filter weights. Feature maps are updated incrementally with *atomic operations*, c.f. algorithm 1, where atomic operations are small enough to be thread-safe, even if no locking mechanism is used. In that

<sup>2</sup>We have also experimented with other sparse formats, like compressed sparse blocks; but found none of them to work as well, mainly due to limitations and idiosyncrasies of current GPU hardware.

respect it is similar to two concurrent works (Parashar *et al.*, 2017; Park *et al.*, 2017). In practice, the incremental update is limited by the current hardware design, since atomic operations are slightly slower than non-atomics: at present, off-the-shelf GPUs do not offer native support for atomic floating point operations in shared memory, although they do for more costly CAS instructions. Yet incremental updating is significantly faster, because it performs only the minimum number of operations necessary to obtain the convolution, while avoiding to multiply or add zeros.

---

#### Algorithm 1 Direct Sparse Convolution with Attention

---

```

1: decompress filter and data indices from 1D to  $kD$ 
2: for  $b \in [0 : batch\_count]$  do
3:   for  $oc \in [0 : out\_channel\_count]$  do
4:     initialize dense buffer with 0
5:     for  $ic \in [0 : in\_channel\_count]$  do
6:       for  $\{id, val\} \in data(b, ic)$  do
7:         for  $\{fid, fval\} \in filter(oc, ic)$  do
8:           compute  $uid$  with get_update_id(id, fid)
9:           atomically add  $val \cdot fval$  to buffer at  $uid$ 
10:        end for
11:       end for
12:     end for
13:     get non-zero entries from buffer
14:     add bias to non-zero entries in buffer
15:     select  $k$  largest responses from non-zero entries
16:     compress ids of  $k$  largest responses from  $kD$  to 1D
17:     write  $k$  largest features and ids as sparse output
18:   end for
19: end for

```

---

The sparse convolution is computed sequentially per output channel and batch, but in parallel across input channels, features and filter weights. Its result is stored in a temporary, dense buffer with dimensions for batches and output channels set to 1, e.g.,  $\{d_b = 1, d_x, d_y, \dots, d_c = 1\}$ . This buffer increases with the resolution of the data, i.e., quadratically for 2D images, cubically for 3D volumes, *etc.*. Still, it is in practice a lot smaller than a typical dense tensor with correct dimensionality for batches and channels, such that volumes up to  $512^3$  can be processed on a single graphics card (Nvidia Titan Xp, 12 GB).

#### 3.2. Preserving sparsity with attention

Convolution with kernels larger than  $(1 \times 1)$  generates fill-in, i.e., it reduces the sparsity of a feature map, by construction. C.f. Figure 2. This “smearing out” of the sparse inputs usually only has a small influence on the output of the network, see section 4.2. But it considerably increases memory consumption and runtime, especially when occurring repeatedly over multiple layers. In order to guarantee upper bounds on the memory footprint and runtime of the network, we

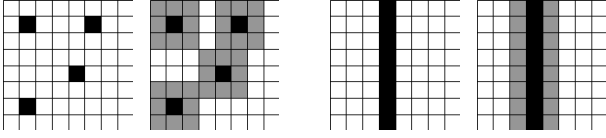


Figure 2. The fill-in (decrease in sparsity) due to convolutions depends on the data distribution. Uniformly distributed data is affected most strongly, e.g., in 3D data every  $3 \times 3 \times 3$  filter would increase the density by a factor of 27, until data is dense.

propose to apply a  $k$ -selection filter on each output channel, keeping only the  $k$  strongest responses. This can be seen as an approximation of the exact convolution output where small responses are suppressed, but using an adaptive threshold that suppresses only as many values as necessary to maintain a desired degree of sparsity.

The parameter  $k$  controls the sparsity, and thus the memory consumption, of the convolutional layers. Processes that aim to optimally direct and manage the limited resources available for some cognitive task are commonly referred to as *attention*. We have implemented two versions of our simple attention mechanism via  $k$ -selection (Alabi et al., 2012): (i) acts on the raw responses, so it prefers large positive responses, making it similar to a rectified linear unit; (ii) picks the  $k$  values with the largest absolute values, expressing a preference for responses with large magnitude. The time complexity of this layer is given by:

$$O((\rho_d \cdot \rho_f \cdot s_f^k \cdot c_{in} + \log(s_d^k)) \cdot s_d^k \cdot c_{out} \cdot b), \quad (1)$$

where  $k$  is the dimension of the data,  $s_d$  its resolution and  $\rho_d$  its density,  $s_f$  denotes the size of the filter and  $\rho_f$  the density of the filter. The number of batches is  $b$  and the number of input and output channels of the layer are  $c_{in}$  and  $c_{out}$ , respectively.

### 3.3. Pooling Layer

Our sparse pooling layer goes through three straight-forward stages. First, features are assigned to an output (hyper-) voxel, by dividing the data channels of their index by strides. Second, the data is sorted w.r.t. voxels, so that all responses within the same voxel are clustered together. Third, the pooling operator is applied separately to each cluster. So far, we have implemented only max-pooling. Clearly, the time complexity of the pooling layer is

$$O(\rho_d \cdot s_d^k \cdot \log(\rho_d \cdot s_d^k) \cdot c_{in} \cdot b). \quad (2)$$

### 3.4. Direct Sparse Backpropagation

Our target for back-propagation is again to skip operations that can be avoided due to sparsity. We must propagate error gradients only to all those features which have produced evidence, in the form of non-zero responses during

the forward pass. Yet, the same performance issues already discussed for the forward pass apply also to the backward pass: back-propagation through a convolutional layer is itself a convolution and therefore produces fill-in, increasing memory use and runtime.

Contrary to the forward pass, it is not advisable to bound the fill-in with the  $k$ -selection technique, since this will not prevent the back-propagated error gradients from spreading to zero activations and vanishing, while smaller gradients flowing towards non-zero activations might be missed. It is evident that this effect could seriously slow down the training process. Hence, we propose to use a stricter back-propagation, which only propagates errors  $L$  to non-zero features  $x$  and model parameters  $w$ :

$$\frac{\partial L}{\partial x_i} = \begin{cases} 0 & \text{for } x_i = 0 \\ \frac{\partial L}{\partial y} \frac{\partial y}{\partial x_i}, & \text{else} \end{cases} \quad (3)$$

$$\frac{\partial L}{\partial w_i} = \begin{cases} 0 & \text{for } w_i = 0 \\ \frac{\partial L}{\partial y} \frac{\partial y}{\partial w_i}, & \text{else} \end{cases} \quad (4)$$

Here, weights are considered equal to zero only if they have been explicitly removed by pruning, so as to avoid suppressing the gradients of weights that pass through  $w_i = 0$  while changing sign. Note the similarity of our approximated back-propagation to the back-propagation through an arbitrary layer with *ReLU* activation function:

$$\frac{\partial L}{\partial x} = \begin{cases} 0 & \text{for } y_i \leq 0 \\ \frac{\partial L}{\partial y'_i} \frac{\partial y_i}{\partial x}, & \text{else} \end{cases}, \quad (5)$$

where  $y_i$  denotes the output of the layer before applying the ReLU and  $y'_i$  denotes the output of the ReLU. Conventional back-propagation sets values to zero in function of the layer output  $y_i$ , whereas we do so as in function of the input features  $x_i$ .

Neglecting zero-elements slightly reduces the efficiency per learning iteration, since not all error gradients are propagated anymore. However, it has a number of advantages: (i) The tensors used for back-propagation have fixed size and shape. Therefore, one can still use optimization frameworks that have been designed for dense data, and expect fixed and known array dimensions; (ii) By considering only gradients on non-zero elements of the forward pass, back-propagation can be implemented in a clean and transparent manner. E.g. for convolutional layers one obtains Algorithm 2, which is very similar to Algorithm 1; (iii) Once a filter weight has been set to zero (see section 3.6 on pruning weights during learning), it will remain zero. Below, we will describe how this property can be used to guarantee that the network gets progressively faster at its task as the learning proceeds and it sees more training data.

**Algorithm 2** Backpropagation for Convolutional Layer

```

1: initialize  $bp\_data$  with  $\text{shape}(\text{input\_values})$  and 0
2: initialize  $bp\_filter$  with  $\text{shape}(\text{filter\_weights})$  and 0
3: decompress filter and data indices from 1D to  $k$ D
4: for  $b \in [0 : \text{batch\_count}]$  do
5:   for  $oc \in [0 : \text{out\_channel\_count}]$  do
6:     initialize dense buffer with  $\text{gradients}(b, oc)$ 
7:     for  $ic \in [0 : \text{in\_channel\_count}]$  do
8:       for  $\{id, val\} \in \text{data}(b, ic)$  do
9:         for  $\{fid, fval\} \in \text{filter}(oc, ic)$  do
10:          compute  $uid$  with  $\text{get\_update\_id}(id, fid)$ 
11:          get gradient  $g$  from buffer at  $uid$ 
12:          atomically add  $g \cdot fval$  to  $bp\_data$  at  $id$ 
13:          atomically add  $g \cdot val$  to  $bp\_filter$  at  $fid$ 
14:        end for
15:      end for
16:    end for
17:  end for
18: end for
    
```

### 3.5. Adaptive density regularisation

The methods in Sections 3.2 and 3.4 directly impose upper bounds on network density. There is, however, a computationally more efficient way to encourage sparsity of the feature maps, such that the sparsity thresholds are rarely exceeded in the first place, and the more costly  $k$ -selection step is avoided. That strategy makes use of the properties of the rectified linear unit (*ReLU*), which is the most popular activation function in modern CNNs. The *ReLU*, by definition, truncates negative activations to zero while leaving positive ones unchanged. This means that we only have to include a regularisation that pushes down the values (not magnitudes) of filter weights (and biases). By doing so, more weights will be driven into the negative region, where they are extinguished by the subsequent *ReLU*. Moreover, the same idea can be used to reduce sparsity when it is not needed, and optimally use the available resources: when too few activations are  $> 0$ , one drives the filter weights up, so that fewer of them are suppressed by the *ReLU*. To achieve the desired effect, we simply add a bias  $b$  to the  $L_2$ -regularisation, so that the regulariser becomes  $\sum(w + b)^2$ . The scalar  $b$  is positive when the density  $\rho$  is too large, and negative when it is overly small:

$$b = \begin{cases} o + b_1 \cdot (\rho - \rho_{up}) & \rho > \rho_{up} \\ & \text{(exceeds available resources)} \\ -b_2 \cdot (\rho_{up} - \rho) & \rho \leq \rho_{up} \\ & \text{(not using available resources)} \end{cases} \quad (6)$$

with  $\rho_{up}$  the upper bound implied by the  $k$ -selection filter, and  $o, b_1, b_2 \geq 0$  control parameters. The offset  $o$  adds an additional penalty for exceeding the available resources,

since this case requires the use of the  $k$ -selection filter and, hence, increases the computational load.

### 3.6. Parameter Pruning

As explained above, our training algorithm has the following useful properties: (i) The regulariser in section 3.5 encourages small model parameters. (ii) The sparse backpropagation in section 3.4 ensures that, once set to zero, model parameters do not reappear in later training steps. Together, these two suggest an easily controllable way to progressively favour sparsity during training: At the end of every training epoch we screen the network for weights  $w$  that are very small:  $|w_i| < \epsilon$ . If the magnitude of a weight  $w_i$  stays low for two consecutive epochs (meaning that it was already close to zero before, and that did not change during one epoch of training) we conclude that it has little influence on the network output and prune it (one-warning-shot pruning). We note that a small weight should not be pruned when first detected, without the ‘‘warning shot’’: it could have a large gradient and just happen to be at its zero-crossing from a large positive to a large negative value (or vice versa) at the end of the epoch. On the contrary, it is very unlikely to observe a weight exactly at its zero-crossing twice in a row in consecutive epochs.

Since a weight, once set to zero, will not reappear with our sparse back-propagation, every pruning reduces the number of non-zero weights, unless all remaining weights have relevant magnitude, in which case their number stays the same. It is thus guaranteed that the network become sparser, and therefore also faster at the task it is learning, as it sees more and more training data, c.f. equation (1). We note, it is well-documented that biological systems get faster at a specific task with longer training (Robertson, 2007; Nissen & Bullemer, 1987).

## 4. Evaluation

In this section we evaluate the impact of upper bounds and regularization on runtime and classification accuracy. The sparse network was implemented into the Tensorflow framework and programmed in C++/CUDA with a python interface. Our experiments were run on PCs with Intel Core i7 7700K processors, 64GB RAM and Titan Xp GPUs. For the evaluation of memory footprint and runtime of our convolutional layer a synthetic dataset of sparse random tensors is used and compared against the dense layers of tensorflow 1.4, which was compiled with Cuda 9.0 and CuDNN 6.0.

We conduct different experiments to evaluate the effects of our sparse network on classification accuracy: First, the impact of upper bounds on classification is evaluated by performing a grid search on the upper bound  $\rho_{up}$  in the

Resolution	$32^3$	$64^3$	$128^3$	$256^3$
Dense [GB]	0.04	0.27	2.15	17.18
Sparse 32 [GB]	$2 \cdot 10^{-3}$	$8 \cdot 10^{-3}$	0.03	-
Sparse 64 [GB]	$3 \cdot 10^{-3}$	0.013	0.05	0.2
Sparse Temp [GB]	$3 \cdot 10^{-4}$	0.002	0.016	0.13

Table 1. Theoretical memory required at different resolutions  $r$  for a convolutional layer with minibatch size 32, output depth 8 and upper bound  $\rho_{up} = \frac{1}{r}$ .

convolutional layers. For this experiment the MNIST data set (LeCun et al., 1998) is used, as it is small enough to perform grid search in a reasonable amount of time and can be interpreted as sparse data (1D lines in 2D images). Second, the effects of pruning on runtime and classification accuracy are shown using the ModelNet data set (Wu et al., 2015a), by varying the strength  $\lambda$  of the regularisation. Modelnet40 provides 3D CAD models of 40 different classes. Furthermore, the classification results of different baseline methods are compared on this data set. Training on Modelnet40 is performed for 90 epochs with a learning rate of 0.001. Minimisation is done by stochastic gradient descent with the *adagrad* optimizer (Duchi et al., 2011).

#### 4.1. Runtime and Memory Footprint

For the evaluation of runtime, convolutions are performed on a sparse voxel grid filled with random numbers. The resolution of the voxel grid  $r^3$  is varied between  $r = 16$  and  $r = 256$ . To achieve the expected data density of a 2D surface in a 3D voxelgrid the data density  $\rho$  as well as the upper bound on the per-channel density  $\rho_{up}$  are set to  $\rho = \rho_{up} = \frac{1}{r}$ . In order to compute the high resolution  $r = 256$  with dense convolutional layers, the mini-batch size and channel size had to be set to one<sup>3</sup>, while the number of output channels was set to 8. The density  $\rho_f$  of the filter weights is varied between 0.1 and 1. As baseline we use the convolutional layer of Tensorflow (Abadi et al., 2016), which performs convolutions via the fast Fourier transform and batched general matrix-matrix multiplication from cuBlas, as front end to cuDNN (Chetlur et al., 2014). We note that processing only a single input channel does not play to the strength of our sparse network. Moreover, Tensorflow is able to use the full capability of the GPU, while our implementation is limited to performing operations in global memory, due to the weak support for atomic floating point operations in shared memory. These advantages are seen especially at small resolutions  $r$  and large densities. In the worst case, at  $r = 32$  tensorflow is  $\approx 9\times$  faster than our implementation. In the best case, at  $r = 256$  and  $\rho_f = 0.1$ , we are  $\approx 14\times$  faster, as shown in Figure 3.

Table 1 shows the memory requirements for dense and

<sup>3</sup>Protobuf limits the size of single tensors to 2 GB.

sparse convolutional layers at various resolutions  $r$ , a mini-batch size of 32, 8 output channels and an upper bound  $\rho_{up} = \frac{1}{r}$ . For our sparse representation we consider both the memory consumption with 64-bit indices and with 32-bit indices. At large resolutions our memory footprint is about two orders of magnitude smaller.

#### 4.2. Contribution of small feature responses

In the context of sparsity the question arises, whether zero-valued features contribute valuable information. Two recent works tried to answer this question. On the one hand, Graham et al. (Graham & van der Maaten, 2017) found that they reach the same accuracies as dense networks for their application, while completely neglecting zero-valued features. On the other hand, Uhrig (Uhrig et al., 2017) concluded that for certain tasks zero-valued features may be beneficial. For our network it is possible to assess the importance of small feature responses (not limited to exact zero-values) by training neural networks with varying upper bounds. For this experiment, CNNs are trained on MNIST for 10 epochs without regularization. The optimization is performed with *adagrad* and a learning rate of 0.01.

The pixels in MNIST were set to zero when their value  $v \in [0, 255]$  was below a threshold of  $v < 50$ , to obtain a sparse dataset with average density  $\overline{\rho_{in}} = 0.23$ , while the upper bound  $\rho_{up}$  ranges from  $\rho_{up} = 0.035$  to  $\rho_{up} = 0.095$ . Note that even though letters can be interpreted as 1D lines in 2D images, the MNIST data has a low resolution of only  $28 \times 28$  pixels. Hence, the data is still not extremely sparse. Except for few outliers, the results in Figure 4a show a slower converges of the training loss with lower upper bounds on the density of the layers. This reduced convergence is caused by dropping some gradients in the backpropagation, as described in section 3.4. However, smaller upper bounds not only guarantee a small memory footprint, but also tend to yield faster runtime, as seen in Figure 4b. The classification results on the test set differ by less than 1.5% between the strictest upper bound and the dense case.

#### 4.3. Regularization and Pruning

With our sparsity-inducing pruning and regularisation, we expect to see faster runtime for stronger regularisers. In order to verify this behaviour, neural networks are trained on Modelnet40 with varying regularisation scales  $\lambda \in \{0, 0.1, 0.2, 0.3\}$ . The bias for density-based regularization is computed with  $b_1 = b_2 = o = 0.1$ . Stronger regularisation decimates the number of (non-zero) filter weights faster, as shown in Figure 5a. It can also be seen that the number of parameters converges when only a fixed set of important weights is left. The drop in non-zero weights also reduces runtime, see Figure 5b.

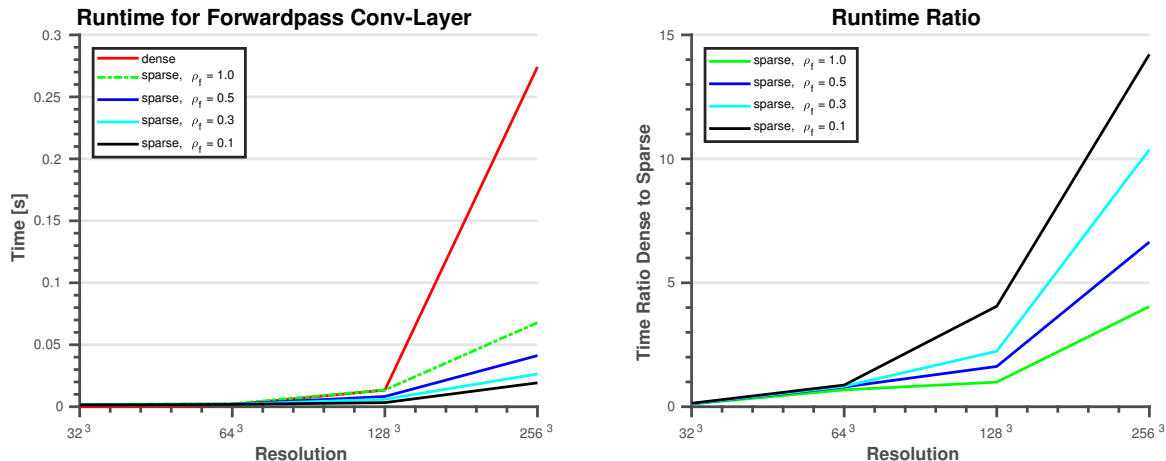


Figure 3. Runtime of a dense convolution layer in Tensorflow and our sparse convolution layer. The runtime (left) and runtime ratio (right) on random sparse input are plotted for different resolutions  $r^3$ . Both the density of the input and the upper bound for the sparse output are set to  $\rho = \rho_{up} = \frac{1}{r}$ . The density of the convolution kernel varies as  $\rho_f \in \{0.1, 0.3, 0.5, 1\}$ . At large resolutions the sparse layer is significantly faster.

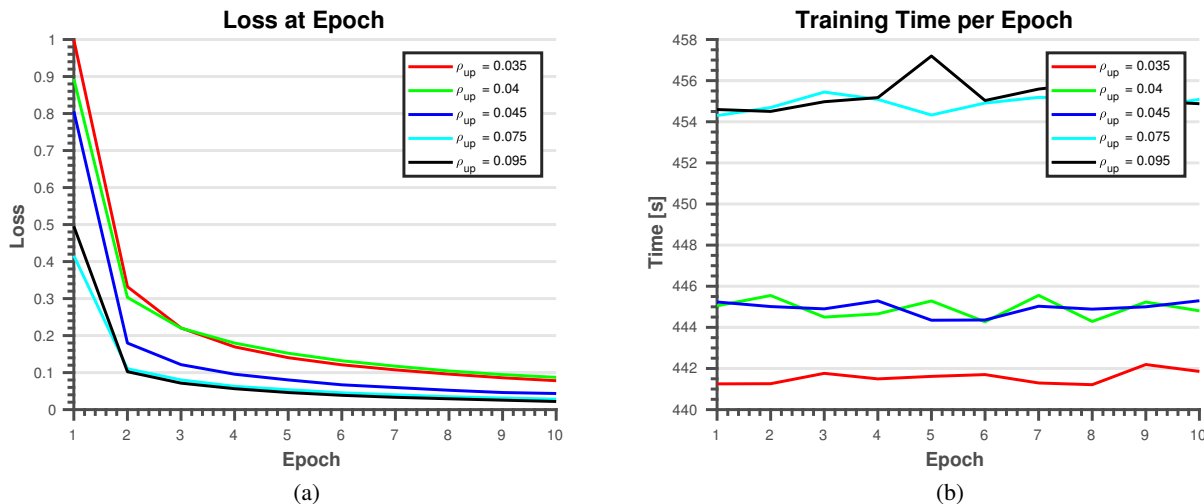


Figure 4. Effect of removing small features with upper bound  $\rho_{up}$ . (a) convergence of the training loss and (b) runtime, measured on the sparse MNIST data set. Stricter upper bounds slow down convergence, but reduce runtime.

After 90 epochs of training, a network regularised with  $\lambda = 0.3$  is 51% faster than one trained without regularisation and pruning, even though only the first nine out of twelve convolutional layers are set to be sparse. Strong regularisation  $\lambda \in \{0.2, 0.3\}$  initially causes an increase in runtime, by driving up the number of non-zero weights to use the available resources via the bias term  $b_2$ . The classification accuracy for all tested regularization scales quickly converges to practically identical values, as shown in Figure 5c. We point out that pruning finds the most suitable sparsity pattern for a given training set. When using a pruned model for transfer learning, it may be safer to re-initialize

the removed filter weights of the sparse representation with zeros before fine-tuning.

#### 4.4. Classification performance on Modelnet40

Finally, we compare our upper-bounded neural network and modified back-propagation against a conventional network. To that end we run OctNet3, a dense network without octree structure, and a sparse version of the same network on Modelnet40, see Figure 6.

First, the input resolution is set to  $r = 16^3$ , while the upper bound on the density is varied between  $\rho_{in} \in$

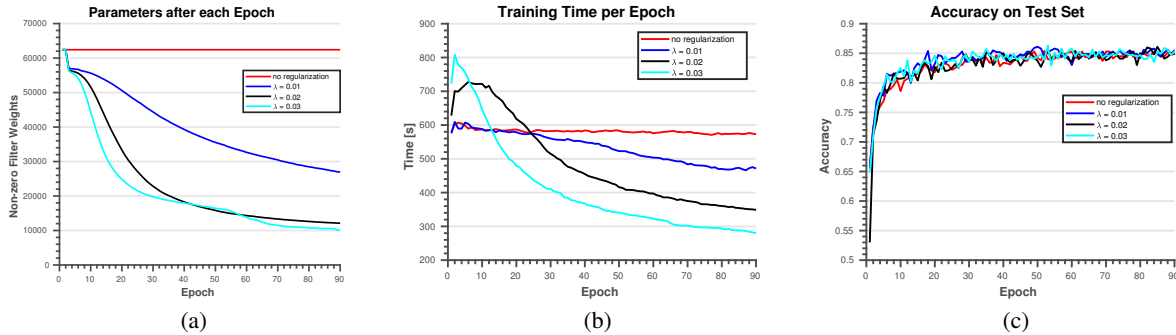


Figure 5. Influence of adaptive density regularisation and pruning on (a) the number of (non-zero) parameters in the convolutional layer, (b) the runtime per training epoch, and (c) the overall accuracy on the Modelnet40 test set. Strong regularisation and pruning significantly reduce the number of parameters and the runtime, without noticeable impact on accuracy.

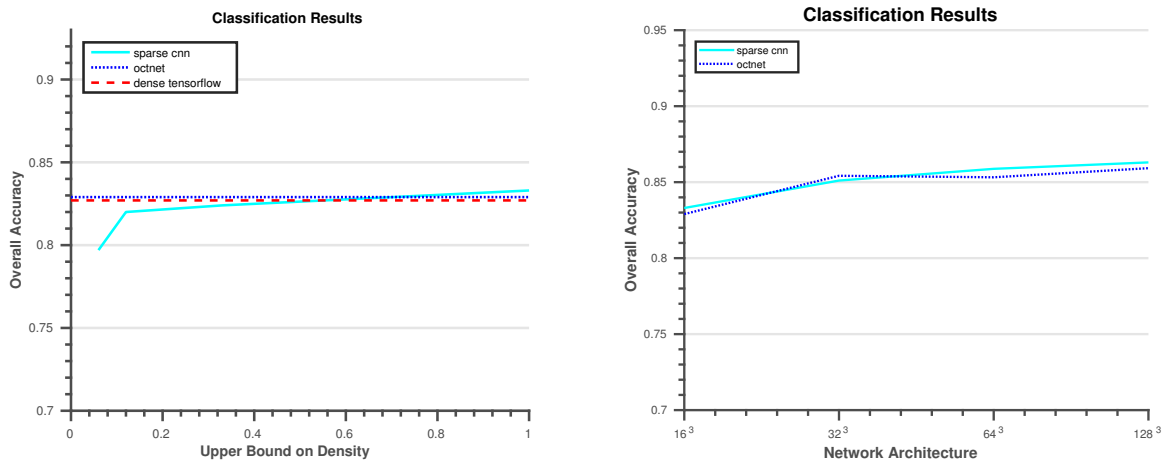


Figure 6. Performance of our sparse network on Modelnet40, compared to two baselines, the equivalent dense network and OctNet. (left) overall accuracy for different upper density bounds; (right) overall accuracy for different input resolutions.

{0.06, 0.12, 0.33, 1.0}. Both, the conventional dense network and Octnet converge to a very similar overall accuracy of  $\approx 0.83$ . For a trivial upper bound  $\rho_{in} = 1.0$  the overall accuracy of our sparse network is also practically the same (in fact slightly better at 0.833, but we attribute this to random fluctuations). Very low upper bounds up to  $\rho_{in} = 0.12$  yield slightly worse results on the  $16^3$  inputs, for the lowest bound  $\rho_{in} = 0.06$  the loss reaches  $\approx 3$  percent points.

Second, the resolution of the input voxel grid is gradually increased:  $r \in \{16^3, 32^3, 64^3, 128^3\}$ . Both the sparse network and OctNet yield similar results, for all resolutions. OctNet performs slightly better on  $r = 32^3$ , while our bounded, sparse network has a small advantage at all other resolutions. Together the two experiments suggest that reasonable upper bounds and our approximated, sparse backpropagation do not negatively impact classification accuracy.

### 5. Conclusion

We have proposed a novel neural network mechanisms which exploit and encourage sparseness in both feature maps and model parameters. At practically useful resolutions, our novel sparse layers and back-propagation rule significantly reduce (i) memory footprint and (ii) runtime of convolutional layers for sufficiently sparse data. Moreover, our approach guarantees upper bounds on the memory requirements and runtime of the network. For classification tasks the performance of our sparse network is comparable to its dense counterpart as well as OctNet. In future work, it will be interesting to employ sparsity also for other tasks. Our implementation is fully compatible with Tensorflow and will be released as open-source code. We hope, that hardware support for sparse convolutions will improve further on future consumer GPUs, as demonstrated by (Parashar et al., 2017); thus further boosting the performance of sparse, high-dimensional CNNs.

## References

- Abadi, Martín, Barham, Paul, Chen, Jianmin, Chen, Zhifeng, Davis, Andy, Dean, Jeffrey, Devin, Matthieu, Ghemawat, Sanjay, Irving, Geoffrey, Isard, Michael, et al. Tensorflow: A system for large-scale machine learning. In *Proceedings of the 12th USENIX Symposium on Operating Systems Design and Implementation (OSDI)*. Savannah, Georgia, USA, 2016.
- Alabi, Tolu, Blanchard, Jeffrey D, Gordon, Bradley, and Steinbach, Russel. Fast k-selection algorithms for graphics processing units. *Journal of Experimental Algorithmics (JEA)*, 17:4–2, 2012.
- Brock, André, Lim, Theodore, Ritchie, James M., and Weston, Nick. Generative and discriminative voxel modeling with convolutional neural networks. *CoRR*, abs/1608.04236, 2016. URL <http://arxiv.org/abs/1608.04236>.
- Chetlur, Sharan, Woolley, Cliff, Vandermersch, Philippe, Cohen, Jonathan, Tran, John, Catanzaro, Bryan, and Shelhamer, Evan. cudnn: Efficient primitives for deep learning. *arXiv preprint arXiv:1410.0759*, 2014.
- Denil, Misha, Shakibi, Babak, Dinh, Laurent, de Freitas, Nando, et al. Predicting parameters in deep learning. In *Advances in Neural Information Processing Systems*, pp. 2148–2156, 2013.
- Denton, Emily L, Zaremba, Wojciech, Bruna, Joan, LeCun, Yann, and Fergus, Rob. Exploiting linear structure within convolutional networks for efficient evaluation. In *Advances in Neural Information Processing Systems*, pp. 1269–1277, 2014.
- Duchi, John, Hazan, Elad, and Singer, Yoram. Adaptive subgradient methods for online learning and stochastic optimization. *Journal of Machine Learning Research*, 12(Jul):2121–2159, 2011.
- Engelcke, Martin, Rao, Dushyant, Wang, Dominic Zeng, Tong, Chi Hay, and Posner, Ingmar. Vote3deep: Fast object detection in 3d point clouds using efficient convolutional neural networks. 2017.
- Graham, Benjamin. Spatially-sparse convolutional neural networks. *arXiv preprint arXiv:1409.6070*, 2014.
- Graham, Benjamin and van der Maaten, Laurens. Submanifold sparse convolutional networks. *arXiv preprint arXiv:1706.01307*, 2017.
- Graham, Benjamin, Engelcke, Martin, and van der Maaten, Laurens. 3d semantic segmentation with submanifold sparse convolutional networks. *CoRR*, abs/1711.10275, 2017. URL <http://arxiv.org/abs/1711.10275>.
- Han, Song, Pool, Jeff, Tran, John, and Dally, William. Learning both weights and connections for efficient neural network. In *Advances in Neural Information Processing Systems*, pp. 1135–1143, 2015.
- Häne, Christian, Tulsiani, Shubham, and Malik, Jitendra. Hierarchical surface prediction for 3d object reconstruction. *CoRR*, abs/1704.00710, 2017. URL <http://arxiv.org/abs/1704.00710>.
- Huang, Jing and You, Suya. Point cloud labeling using 3d convolutional neural network. In *Proc. of the International Conf. on Pattern Recognition (ICPR)*, volume 2, 2016.
- Jaderberg, Max, Vedaldi, Andrea, and Zisserman, Andrew. Speeding up convolutional neural networks with low rank expansions. *CoRR*, abs/1405.3866, 2014. URL <http://arxiv.org/abs/1405.3866>.
- Karpathy, Andrej, Toderici, George, Shetty, Sanketh, Leung, Thomas, Sukthankar, Rahul, and Fei-Fei, Li. Large-scale video classification with convolutional neural networks. In *Proceedings of the IEEE conference on Computer Vision and Pattern Recognition*, pp. 1725–1732, 2014.
- Krizhevsky, Alex, Sutskever, Ilya, and Hinton, Geoffrey E. ImageNet classification with deep convolutional neural networks. In *NIPS*, 2012.
- Lai, Kevin, Bo, Liefeng, and Fox, Dieter. Unsupervised feature learning for 3d scene labeling. In *Robotics and Automation (ICRA), 2014 IEEE International Conference on*, pp. 3050–3057. IEEE, 2014.
- LeCun, Yann, Bottou, Léon, Bengio, Yoshua, and Haffner, Patrick. Gradient-based learning applied to document recognition. *Proceedings of the IEEE*, 86(11):2278–2324, 1998.
- Li, Yangyan, Pirk, Sören, Su, Hao, Qi, Charles R., and Guibas, Leonidas J. Fpnn: Field probing neural networks for 3d data. In Lee, D. D., Sugiyama, M., Luxburg, U. V., Guyon, I., and Garnett, R. (eds.), *Advances in Neural Information Processing Systems*, volume 29, pp. 307–315, 2016.
- Liu, Baoyuan, Wang, Min, Foroosh, Hassan, Tappen, Marshall, and Pensky, Marianna. Sparse convolutional neural networks. In *Proceedings of the IEEE Conference on Computer Vision and Pattern Recognition*, pp. 806–814, 2015.
- Long, Jonathan, Shelhamer, Evan, and Darrell, Trevor. Fully convolutional networks for semantic segmentation. In *IEEE Conference on Computer Vision and Pattern Recognition*, pp. 3431–3440, 2015.
- Maturana, Daniel and Scherer, Sebastian. Voxnet: A 3d convolutional neural network for real-time object recognition. In *Intelligent Robots and Systems (IROS), 2015 IEEE/RSJ International Conference on*, pp. 922–928. IEEE, 2015.
- Nissen, Mary Jo and Bullemer, Peter. Attentional requirements of learning: Evidence from performance measures. *Cognitive psychology*, 19(1):1–32, 1987.
- Parashar, Angshuman, Rhu, Minsoo, Mulkara, Anurag, Puglielli, Antonio, Venkatesan, Rangharajan, Khailany, Brucek, Emer, Joel, Keckler, Stephen W, and Dally, William J. Scnn: An accelerator for compressed-sparse convolutional neural networks. In *Proceedings of the 44th Annual International Symposium on Computer Architecture*, pp. 27–40. ACM, 2017.
- Park, Jongsoo, Li, Sheng, Wen, Wei, Tang, Ping Tak Peter, Li, Hai, Chen, Yiran, and Dubey, Pradeep. Faster cnns with direct sparse convolutions and guided pruning. In *Proc. of the International Conf. on Learning Representations (ICLR)*, 2017.
- Prokhorov, Danil. A Convolutional Learning System for Object Classification in 3-D Lidar Data. *IEEE Transactions on Neural Networks*, 21(5):858–863, 2010.
- Qi, Charles R., Su, Hao, Mo, Kaichun, and Guibas, Leonidas J. Pointnet: Deep learning on point sets for 3d classification and segmentation. In *IEEE Conference on Computer Vision and Pattern Recognition*, 2017a.

- Qi, Charles R., Yi, Li, Su, Hao, and Guibas, Leonidas J. Pointnet++: Deep hierarchical feature learning on point sets in a metric space. 2017b.
- Ren, Shaoqing, He, Kaiming, Girshick, Ross, and Sun, Jian. Faster R-CNN: Towards real-time object detection with region proposal networks. In *NIPS*. 2015.
- Riegler, Gernot, Ulusoy, Ali Osman, and Geiger, Andreas. Octnet: Learning deep 3d representations at high resolutions. In *Computer Vision and Pattern Recognition (CVPR), 2017 IEEE Conference on*. IEEE, 2017.
- Robertson, Edwin M. The serial reaction time task: implicit motor skill learning? *Journal of Neuroscience*, 27(38):10073–10075, 2007.
- Song, Shuran and Xiao, Jianxiong. Deep sliding shapes for amodal 3d object detection in rgb-d images. In *Proceedings of the IEEE Conference on Computer Vision and Pattern Recognition*, pp. 808–816, 2016.
- Tatarchenko, Maxim, Dosovitskiy, Alexey, and Brox, Thomas. Octree generating networks: Efficient convolutional architectures for high-resolution 3d outputs. 2017.
- Uhrig, Jonas, Schneider, Nick, Schneider, Lukas, Franke, Uwe, Brox, Thomas, and Geiger, Andreas. Sparsity invariant cnns. *arXiv preprint arXiv:1708.06500*, 2017.
- Wen, Wei, Wu, Chunpeng, Wang, Yandan, Chen, Yiran, and Li, Hai. Learning structured sparsity in deep neural networks. In *Advances in Neural Information Processing Systems*, pp. 2074–2082, 2016.
- Wu, Zhirong, Song, Shuran, Khosla, Aditya, Yu, Fisher, Zhang, Linguang, Tang, Xiaoou, and Xiao, Jianxiong. 3d shapenets: A deep representation for volumetric shapes. In *Proceedings of the IEEE Conference on Computer Vision and Pattern Recognition*, pp. 1912–1920, 2015a.
- Wu, Zhirong, Song, Shuran, Khosla, Aditya, Yu, Fisher, Zhang, Linguang, Tang, Xiaoou, and Xiao, Jianxiong. 3d shapenets: A deep representation for volumetric shapes. pp. 1912–1920, 2015b.

## Appendix

### A. Memory requirements

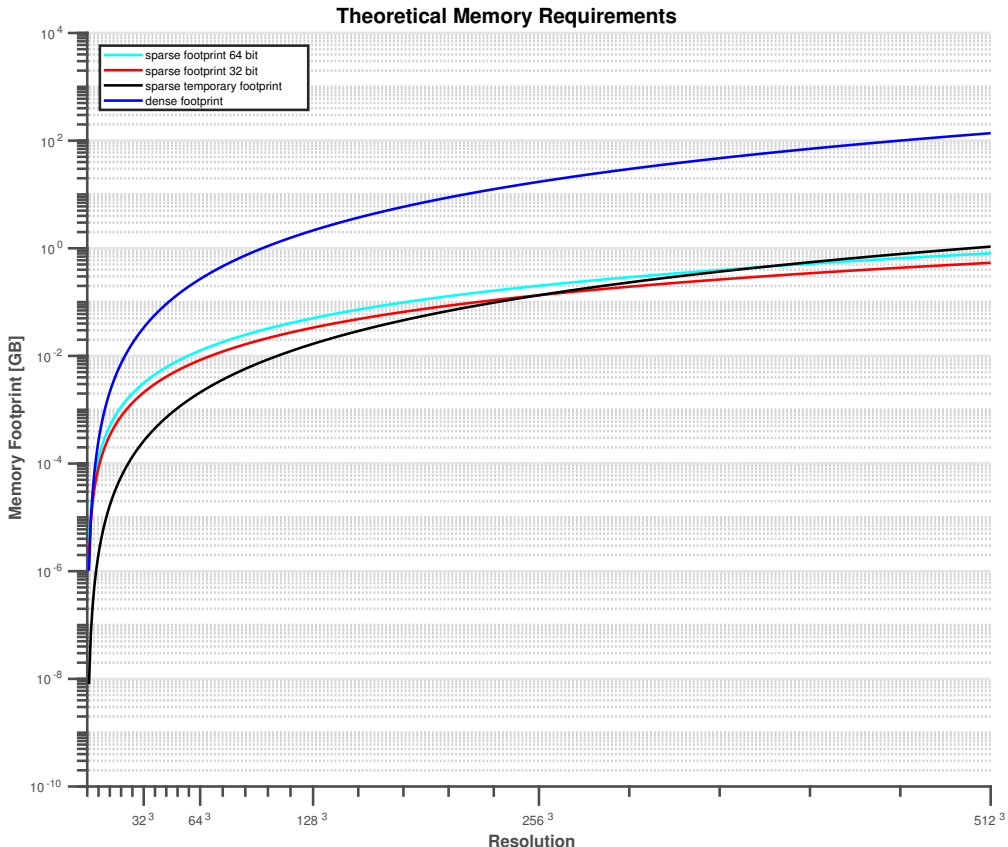


Figure 7. The theoretical memory requirements for the forward pass of a sparse and a dense layer for different resolutions with a minibatch size of 32 and 8 output channels. The upper bound on density is set to:  $\rho_{up} = \frac{1}{res}$ . The size of the input tensor is neglected, so that only the temporary tensors and result of the convolutional layer are considered.

Figure 7 shows the memory footprint of the feature maps for the first convolutional layers of Table 2, where the resolution  $r$  is varied, the minibatch size is set to 32, the number of output channels is set to 8 and the upper bound on density is set to  $\rho_{up} = \frac{1}{r}$ . Dense convolutions require only a single output tensor. The sparse case depends on tensors for indices and data as well as a temporary buffer, which can be reused in all layers. For this experiment the data type is a 32 bit floating point type and two index types are considered: 32 bit and 64 bit. Note that in our implementation 32 bit indices can only be used for resolutions  $r < 256^3$  due to buffer overflows. In general our sparse representation requires less memory than dense for the chosen settings. Especially, at the largest resolutions of  $r = 512^3$  requires 170 times less memory than dense tensors, so that it becomes feasible to even work with large resolutions up to  $r = 512^3$ .

### B. Network Architectures

Table 2 shows the network architectures of our experiments. For our experiments we used the following network parameters: Section 4.2) The experiments on MNIST have  $c = 10$  classes and deployed OctNet3-24<sup>2</sup> with:  $\rho_{21}$  being specified in the text and  $\rho_{22} = 2 \cdot \rho_{21}$ .

The following experiments on Modelnet40 deploy  $c = 40$  distinct classes:

OctNet3-16 <sup>3</sup>	OctNet3-24 <sup>2</sup>	OctNet3-32 <sup>3</sup>	OctNet3-64 <sup>3</sup>	OctNet3-128 <sup>3</sup>	OctNet3-256 <sup>3</sup>
conv(1, 8, $\rho_{11}$ ) conv(8, 8, $\rho_{11}$ ) conv(8, 8, $\rho_{11}$ ) maxPooling(2)	conv(1, 8, $\rho_{21}$ ) conv(8, 8, $\rho_{21}$ ) conv(8, 8, $\rho_{21}$ ) maxPooling(2)	conv(1, 8, $\rho_{31}$ ) conv(8, 8, $\rho_{31}$ ) conv(8, 8, $\rho_{31}$ ) maxPooling(2)	conv(1, 8, $\rho_{41}$ ) conv(8, 8, $\rho_{41}$ ) conv(8, 8, $\rho_{41}$ ) maxPooling(2)	conv(1, 8, $\rho_{51}$ ) conv(8, 8, $\rho_{51}$ ) conv(8, 8, $\rho_{51}$ ) maxPooling(2)	conv(1, 8, $\rho_{61}$ ) conv(8, 8, $\rho_{61}$ ) conv(8, 8, $\rho_{61}$ ) maxPooling(2)
conv(8, 16, $\rho_{12}$ ) conv(16, 16, $\rho_{12}$ ) conv(16, 16, $\rho_{12}$ ) sparseToDense(c)	conv(8, 16, $\rho_{22}$ ) conv(16, 16, $\rho_{22}$ ) conv(16, 16, $\rho_{22}$ ) sparseToDense(c)	conv(8, 16, $\rho_{32}$ ) conv(16, 16, $\rho_{32}$ ) conv(16, 16, $\rho_{32}$ ) maxPooling(2)	conv(8, 16, $\rho_{42}$ ) conv(16, 16, $\rho_{42}$ ) conv(16, 16, $\rho_{42}$ ) maxPooling(2)	conv(8, 16, $\rho_{52}$ ) conv(16, 16, $\rho_{52}$ ) conv(16, 16, $\rho_{52}$ ) maxPooling(2)	conv(8, 16, $\rho_{62}$ ) conv(16, 16, $\rho_{62}$ ) conv(16, 16, $\rho_{62}$ ) maxPooling(2)
		conv(16, 24, $\rho_{33}$ ) conv(24, 24, $\rho_{33}$ ) conv(24, 24, $\rho_{33}$ )	conv(16, 24, $\rho_{43}$ ) conv(24, 24, $\rho_{43}$ ) conv(24, 24, $\rho_{43}$ ) sparseToDense(c)	conv(16, 24, $\rho_{53}$ ) conv(24, 24, $\rho_{53}$ ) conv(24, 24, $\rho_{53}$ ) sparseToDense(c)	conv(16, 24, $\rho_{63}$ ) conv(24, 24, $\rho_{63}$ ) conv(24, 24, $\rho_{63}$ ) sparseToDense(c)
			maxPooling(2) conv(24, 32) conv(32, 32) conv(32, 32)	maxPooling(2) conv(24, 32) conv(32, 32) conv(32, 32)	maxPooling(2) conv(24, 32) conv(32, 32) conv(32, 32)
				maxPooling(2) conv(32, 40) conv(40, 40) conv(40, 40)	maxPooling(2) conv(32, 40) conv(40, 40) conv(40, 40)
					maxPooling(2) conv(40, 48) conv(48, 48) conv(48, 48)
dropout(0.5) fully-connected(1024) fully-connected(c)					

Table 2. For evaluation of our sparse network we use the OctNet3 network architectures similar to the architectures proposed by Riegler et al.

Section 4.3) The regularization experiment deploys OctNet3-64<sup>3</sup> with  $\rho_{41} = 0.06$ ,  $\rho_{42} = 0.14$ ,  $\rho_{43} = 0.33$ ,  $\epsilon = 0.01$ .

Section 4.4 a) Figure 6 (left) uses OctNet3-16<sup>3</sup> with various upper bounds:  $\rho_{11} = \{0.06, 0.12, 0.33, 1\}$ ,  $\rho_{12} = \{0.12, 0.24, 0.33, 1\}$ .

Section 4.4 b) In Figure 6 (right) the following networks are used: OctNet3-16<sup>3</sup> with  $\rho_{11} = \rho_{12} = 1$ ; OctNet3-32<sup>3</sup> with  $\rho_{31} = 0.14$ ,  $\rho_{32} = 0.33$ ,  $\rho_{33} = 0.66$ ; OctNet3-64<sup>3</sup> with  $\rho_{41} = 0.06$ ,  $\rho_{42} = 0.14$ ,  $\rho_{43} = 0.33$ ; OctNet3-128<sup>3</sup> with  $\rho_{51} = 0.02$ ,  $\rho_{52} = 0.06$ ,  $\rho_{53} = 0.14$ .

### C. Sparseness in Modelnet40 Data

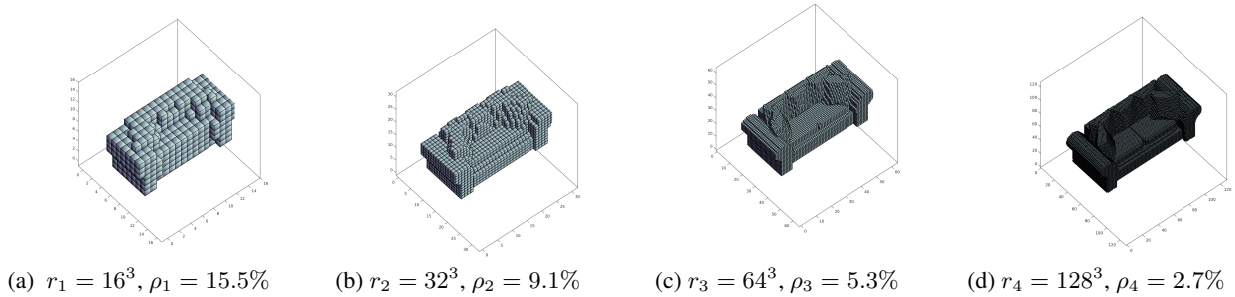


Figure 8. Effects of voxelization  $r$  on density  $\rho$  in voxel grid on example from Modelnet40

Figure 8 shows the effects of different voxel-sizes on the density in the voxel grids. The density of the voxelgrids increases with coarser voxelization. Note that the data does not represent typical line-of-sight measurements, since there are non-zero voxels located on facets *inside* the couch.